v. 5, n. 2, 2025

Journal of Engineering Research

IMPLEMENTATION OF A QC PROCEDURE BASED ON THE ABSOLUTE DOSIMETRY OF ^{192}IR-HDR SOURCES BY μ-IONIZIATON CHAMBER

Acceptance date: 03/02/2025

Miguel Martinez-Albaladejo
Radiotherapy Physics

Abstract: The purpose of this report is to establish a method for the direct measurement of the absorbed dose delivered by ^{192}Ir high--dose-rate (HDR) brachytherapy (BT) sources using a PinPoint ionization chamber. After a literature review, a quality control procedure for the absorbed dose-in water has been developed and included in the quality assurance (QA) of the brachyhterapy unit GammaPlus iX (Varian Medical Systems, Palo, CA).

INTRODUCTION

Treatment planning and dosimetry in brachytherapy have not developed at the same pace as that of external beam radiotherapy (EBRT). Traditionally, there has been a high dependence on clinical experience gained over many years, using known, non-optimised BT systems. Additionally, there have not been any very accurate dosimetry systems for use with BT. This has meant that the same relatively simple algorithms and calculation procedures have been in use for many years and the tolerances on dosimetry have consequently been greater than those accepted for EBRT.

The methodology for quantifying the strength of a BT source in terms of air kerma strength (S_K) measurement as well as the established dosimetry protocols for dose rate calculations around such a source based on its strength, have been extensively discussed in many procedures and literature references[1–5]. For the determination of the different parameter values implemented in the internationally established TG-43[6] and TG-43U[7] dosimetry protocol experimental validation of MC simulation results is required[8]. This applies to both the dose rate constant (Γ) that requires measurement of the absolute dose or dose rate, as well as the radial dose function g(r) and anisotropy function F(r,θ) which are relative values. Furthermore, the need to investigate and quantify the dose perturbation arising from simple or complex applicator geometries and applicator materials, shielding materials, and tissue inhomogeneities, also requires the availability of appropriate experimental dosimetry systems in modern BT[8].

There has also recently been increased interest in improved accuracy of BT dosimetry due to:

- The advent of remote afterloading using HDR and LDR sources.
- The increased availability of CT and MRI scan data for volume definition.
- The possibilities of real-time dosimetric and biological optimisation.

For the above reasons, it is necessary to assess the accuracy of dose delivery as an advanced step with regards to the conventional measurements of the air-kerma strength of a BT source.

LITERATURE REVIEW

The radiation field around BT sources is characterized by: (1) high dose gradients, (2) an extended dose rate range, and (3) photon energies typically lower than those in the standardized dosimetry of external beam fields, which spreads from those of high (^{60}Co and ^{137}Cs) and intermediate (^{198}Au, ^{192}Ir, and ^{169}Yb), to those of low energy radionuclides (^{125}I and ^{103}Pd). Given these three characteristics of the radiation field, experimental BT dosimetry places severe demands on candidate detectors, which are collected in Table 1.

The size of a detector defines both the maximum **spatial resolution** that can be achieved as well as the mini- mum meaningful distance of measurement. Especially in intermediate and high energy radionuclides, a softening of the photon spectrum is observed with increased distance from the source due to the gradual build-up of scattered (Compton effect), lower energy photons and the attenuation of the primary emitted photons (see Fig.1). Owing to this energy softening effect, the **energy response** of a detector becomes crucial with regards its suitability for experimental studies (Fig.2). Finally, pronounced **anisotropic angular** response of detectors is expected to lead to underestimation of the dose with increased distance from the source since the fraction of backscattered photons increases with distance.

There is a variety of experimental dosimeters that have been used for dosimetry around BT sources, such as ion- ization chambers[9–11], thermoluminescence dosimetry (TLD)[12–21], diodes[22–23], plastic scintillators[24–26], diamond detectors[27–29], radiographic and radiochromic films[30–34], polymer gels and chemical dosimeters[35–45].

Ionization chambers, diodes, plastic scintillators, and diamond detectors have the advantage of allowing direct measurement in phantoms, thus obviating the need for solid-state phantoms and the influence of corresponding corrections and their associated uncertainties. On the other hand, LiF thermoluminescence dosimetry is currently the method of choice for both absolute and relative dose measurement in the entire energy range of BT sources.

BT Difficulty	Requested Feature of the Detector
Simultaneous measure of high and low doses	Great dynamic measure interval
Energetic spectrum dependent of the detector position	Flat energy response
Detector perturbation in the medium (attenuation...)	Water equivalent detector
Average active volume effect in the detector	Very small detector
Very low doses	High sensitivity
Spatial anisotropy of emissions with non uniform distribution of activity	Isotropic response
High gradients and distances source-detector	Accurate positioning

Table 1: Difficulties in experimental brachytherapy

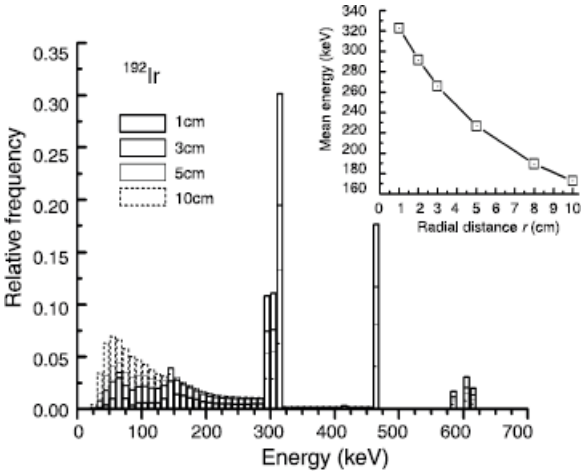

Fig.1. *Photon energy spectra in liquid water at radial distances in the range 1.0 to 10.0cm from a ideal point sources of ^{192}Ir. These are the results of MC calculations with the MCNP-4c MC general code[45] where the source was located in the center of a liquid water spherical phantom of an external radius of 80.0 cm. A maximum number of 2 ·10^8 particle histories were initiated resulting in a maximum relative percentage deviation less than 0.1%. The decrease of the mean energy with the distance from the source is shown.*

DETECTOR CHOICE

The radiation detector **PinPoint PTW31016** (S.N. 00551) has been chosen for this study. With the use of this rigid ionization chamber, a compromise between the properties of sensitivity, volume averaging and anisotropic effects is reached, and the other requirements presented in Table 1 are also satisfied.

In general, ionization chambers can be used in either water phantoms or solid material phantoms for the measurement of relative dose distributions, as well as of absolute dose and dose rate values in BT. Ionization chambers with small dimensions and thus of small collecting volumes, usually in the range 0.01 to 0.6 cm^3, should be considered in order to achieve appropriate spatial resolution[47–50] and keep dose gradient-related effects (volume averaging) at an acceptable level. Thus, an optimum chamber volume has to be selected to achieve, on the one hand, adequate **spatial resolution** (the smaller the volume the better), and on the other hand, a proper **chamber signal** (the larger the volume the better). In our scenario, this is satisfied with a sensible volume of 0.015 cm^3. Depending on the source strength and due to their small collecting volume, certain restrictions will be placed on the maximum possible measurement distance, which will result in proper chamber readings.

Chambers with the lowest possible **energy dependence** in their response at the energy region of interest should be considered, especially for intermediate energy radionuclides, such as ^{192}Ir where a clear energy softening effect is expected. This effect in modern thimble chambers is marginal[51] and will be quantified in the next section. Additionally, the chosen chamber should demonstrate a **flat angular** response over the angle range relevant to the experimental set-up in order to reduce possible positional errors. In this sense, the directional response of the chosen detector was tested in a Varian CLINAC 2100 iX. The chamber was inserted into the ArcCHECK cavity plug accessory, so as the effective point is at the machine isocenter. 5x5 cm^2 field sizes at the isocenter were set with 6 MV as nominal accelerator potential. The tilting of the axis was varied rotating the couch, according to non-coplanar beams, up to the angle (θ) of ± 90° with regards to the natural couch axis. The deviations regarding no tilting were compared with the 1% of the specified tolerances (up 110°). Each measurement is taken in relative as the average of 3 readings for 100 monitor units (MU) as follows below:

Mean readings (div) and deviations (%) regarding no rotation (θ = 0°)				
θ=0°	θ = 30°	θ = 60°	θ = 90°	θ = -30
3.070 (0.0)	3.080 (0.3)	3.080 (0.3)	3.100 (1.0)	3.067 (-0.2)

DOSIMETRY FORMALISM

REFERENCE MEDIUM

The reference medium for dosimetry of BT sources is water[7,51,52].

Given that the accuracy in source-detector positioning is crucial in dosimetry of BT sources due to the high dose gradients in their vicinity, **solid phantoms** that can be precisely machined have also been considered for use with other kinds of detectors, such as ionization chambers, for intermediate and high energy radionuclides[51,52].

Experimental dosimetry in solid phantoms is more convenient than in water due, firstly, to the high degree of geometrical accuracy and, thus, reproducibility, and, secondly, as commonly available ionization chambers in radiotherapy departments can be used without any need for additional accessories or QA procedures. However, the dosimetric characteristics of these materials depend on the energy spectrum of the emitted photons. Furthermore, owing to the energy softening effect with increasing distance from a sour-

ce (Fig.1), the dosimetric characteristics of a specific phantom material are expected to be distance dependent, like in water.

What is of practical interest is the correction required for absorption and scattering of the radiation at a specific radial distance from a source in a phantom when compared with liquid water, $k_{m,w}$, that can be calculated using:

$$k_{m,w}(r) = \frac{\dot{D}_m(r)}{\dot{D}_w(r)} \qquad (1)$$

where $\dot{D}m(r)$ is the dose rate to water in a medium (phantom material) per unit source strength at a distance r from the source and $\dot{D}w(r)$ is the dose rate to water in water per unit source strength at the same distance. Although the energy shifting effect is generally distance and polar angle dependent for cylindrical sources which is specially the case for the intermediate and high energy radionuclides, for reasons of simplification only the radial distance dependence is considered herein. This simplification, however, does not significantly influence or limit the results of the following discussion[4].

Simulations coded in MCNP-4c MC[45] show this correction factor for several phantom materials (Fig.2). The phantom used in this study is composed by WTe material whose standard density is 1.040 (IPEMB, 1996):

PROPOSED FORMALISM

The estimate of the required dose to water in water, D_w, from the ionization chamber reading depends on the available calibration factor N of the chamber used.

The most commonly used calibration protocol for ionization dosimetry in radiotherapy is that of dose to water in water[52–61]. Thus, for most ionization chambers available in radiotherapy departments, calibration factors are expressed in terms of dose to water in water, N_w, for a reference beam quality available. While ^{60}Co beams are usually considered as the reference quality, our chamber will be **cross-calibrated** in terms of air kerma and X-Rays (XR) beams. This procedure will be described in the following section.

Absorbed dose

In general, the dose to water in water medium, D_w, expressed in Gy can be determined from the detector measure- ment M in a medium m (phantom material) using the following equations[4](*pp.448-451*):

$$D_w = DCF \cdot M \cdot ACF \quad , \qquad (2)$$

$$DCF = [N_{K,Q}^{cross} \cdot k_{ch,Q}] \cdot k_\rho \cdot k_{ion} \cdot k_{ph} \cdot (1 - g_\alpha) \cdot \left(\frac{\mu^{en}}{\rho}\right)_\alpha^w \approx [N_{K,Q}^{cross} \cdot k_{ch,Q}] \cdot k_\rho \cdot k_{ion} \cdot k_{ph} \cdot \left(\frac{\mu^{en}}{\rho}\right)_\alpha^w , \qquad (3)$$

$$[N_{K,Q}^{cross} \cdot k_{ch,Q}] = [N_{K,Q_0}^{cross} \cdot k_{ch,Q_0}] \cdot k_{Q,Q_0} \cdot k_V \cdot k_{\alpha p}, \qquad (4)$$

where:

$N_{k,Q}^{cross}$: is the air kerma calibration coefficient of the chamber for the specific energy of the radionuclide considered, Q , expressed as: $N_{k,Q}^{cross} \equiv N_{K,Q_0}^{cross} \cdot k_{Q,Q_0}$ [Gy/div]. The term N_{K,Q_0}^{cross} refers to the coefficient determined at the inter-comparison quality Q_0. For ^{192}Ir sources, simplified concepts exist for the estimation of the second above factors. The BIR/IPSM recommends that the calibration factor for the highest available kilovoltage quality, heavily filtered XR is used (Half Value Layer-HVL- is 2.04mmCu) and, in addition, a general correction of 3% per gcm^{-2}of low atomic number material (plastic or graphite) and for small thicknesses is to be considered[52]. According to the PTW detectors catalogue: Total Wall Area Density (PMMA+graph)= 0.085 g/cm^2, so the quality correction is:

$$k_{Q,Q_0} = 1 + 0.03 \cdot (Wall\ Area\ Density) = 1 + 0.03 \cdot 0.085 \approx 1.00255. \qquad (5)$$

The reader should note that the alternative of extrapolating the calibration coefficient from HVL curves is not contemplated here given the substantial differences between the BT and XR photon spectra.

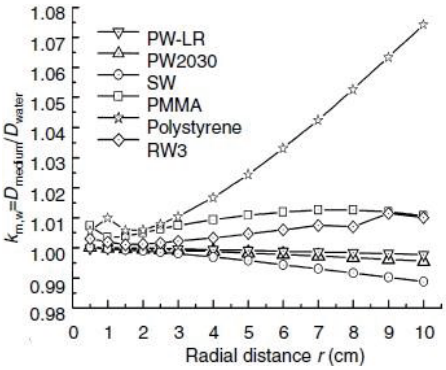

Material	Density ρ (g cm^{-3})	Mean Ratio of Atomic Number to Atomic Mass $\langle Z/A \rangle$	$\rho\langle Z/A \rangle$	Z_{eff}
Plastic water (PW or PW2030)	1.022	0.540468	0.552	6.60
Plastic water (PW-LR)	1.029	0.538155	0.554	6.65
Solid water	1.017	0.539470	0.549	6.36
Polymethyl methacrylate (PMMA)	1.190	0.539369	0.642	6.24
Polystyrene	1.060	0.537680	0.570	5.61
RW3	1.045	0.536452	0.561	5.83
Water liquid H_2O	1.000	0.555087	0.555	7.22

Fig.2. *Correction factor depending on the radial distance r from a point source in a phantom when compared with liquid water, km,w* , according to (1). Five phantom materials, plastic water (PW-LR and PW2030), solid water(SW), PMMA, Polystyrene and RW3, have been considered. These are MC simulation calculation results for ^{192}Ir, where the point sources were located in the center of a liquid water spherical phantom of an external radius of 80.0 cm achieving practically an unbounded geometry. A maximum number of 2 ·10^8 particle histories were initiated for MC simulation study resulting in a maximum relative percentage deviation of 1σ less than 0.1%.

- $\mathbf{k}_{ch,Q}$: includes the **overall perturbation factor** of the chamber at Q, taking into account the changes in the response of the chamber due to the differences when changing from a surrounding medium of air to one of a phantom material. This factor is chamber type dependent and typically estimated by Monte Carlo (MC)[58]. For XR, $k_{ch,Q0}$ will be included in the procedure of cross-calibration.

- $\mathbf{k}_{\alpha,p}$: would correct the previous overall perturbation factor when considering the quality Q instead of Q_0 (idea considered in $k_{ch,Q0}$) and disregarding the effect of the chamber finite size (included in the forthcoming factor k_V). Since the phantoms used for the inter-comparison and BT measurements are quite similar, a good approximation is: [$k_{\alpha,p}$= 1.00][51,53].

- $\mathbf{k}_V$: is a correction factor to account for the effect of the **chamber's finite size** when the center of the cham- ber air cavity volume is considered as the point of reference. It can be estimated by Kondo and Randolph theory applied in our detector geometry[65]: Length = Radius = 1.45 mm, r = 4.75cm → k_V = 1.0004 ≈ 1.000 (side- ways irradiation, which is the predominant one in our geometry).

- **M**: is the **measured charge** (C) during the integration interval time.

- **ACF**: is the **air density** correction factor for the current air and pressure conditions P,T, expressed in hPa and K, other than that referred in the calibration protocol of the reference Farmer chamber -1013.25 hPa and 293.15 K, respectively. It is proportional to (T+273.15) and inversely proportional to P.

- $\mathbf{k}_\rho$: is the correction factor for the **polarity effect** of the bias voltage for the photon energy of the radionuclide, not negligible in small volume chambers[67]. It can be expressed as follows[53,67]:

$$k_\rho = \frac{k_{\rho,^{192}Ir}}{k_{\rho,XR}} \qquad (6)$$

$$k_{\rho,Q} = \left(\frac{|M_1| + |M_2|}{2|M_1|}\right)_Q \quad , \qquad (7)$$

where $M_1$and M_2 are the measured signals of the chamber for the standard and inverse voltage, respectively.

- $\mathbf{k}_{ion}$: is the correction factor that accounts for the unsaturated ion collection efficiency and thus for the charge lost to **recombination** for the specific radionuclide photon energy and the applied nominal voltage V. The recombination

factor for both BT and XR scenarios are calculated as the reciprocal of the ion collection efficiency according to the continuous radiation theory[63,64,67]:

$$k_{ion} = \frac{k_{ion,^{192}Ir}}{k_{ion,XR}} \qquad (8)$$

$$k_{ion,^{192}Ir} = \frac{3}{4 - M/M_2}; \quad k_{ion,XR} = \frac{3}{4 - M/M_2} \ , \qquad (9)$$

with M the collected charge at the nominal voltage V and M_2, at V/2.

- $\mathbf{k}_{p,h}$: is the correction required for absorption and scattering of the radiation at the specific point of mea- surement in our **phantom**. In general, this factor is distance and polar angle dependent, so it has to be estimated experimentally or using MC simulation calculations for the specific measurement set-up. Details for estimating $k_{p,h}$ in our geometry are given in Appendix 5.

- $\mathbf{g}_{\alpha}$: is the energy fraction of the electrons which are liberated by photons in air that are lost due to **bremsstrahlung**. For our relevant photon qualities is negligible[4](table 7.9).

- $\left(\frac{\mu^{en}}{\rho}\right)_{\alpha}^{w}$: is the ratio of **mass energy absorption coefficient** of water to that of air. Literature value is: 1.111 (at E_{eff} [^{192}Ir])[4](table 7.15).

Dose-rate estimation

The formalism based on equation (2) also permits the calculation of the **dose rate** values, $D^{\cdot}w$, using:

$$D_w(\vec{r}) = \int_{t_0=0}^{t} \dot{D}_w(, t_0) e^{-\lambda(t'-t_0)}\, dt' = \dot{D}_w \cdot t \ , \qquad (10)$$

with **t** the interval of integration of charge in the electrometer in which the source is irradiating.

The expression (10) comes from the approximation: $t \ll \frac{1}{\lambda_{(192Ir)}} \approx 154000\ min \rightarrow \ 1 - e^{-t\cdot\lambda_{(^{192}\mathrm{Ir})}} \approx t \cdot \lambda_{(192Ir)}$.

CROSS-CALIBRATION PROCEDURE

The cross-calibration has been performed between the field detector (ionization chamber PinPoint-PP) and the reference detector with traceability to the NPL secondary standard (NE2611-SS), in a Gulmay XStrahl machine. The electrometers connected to the PP have been UNIDOS Brachy, 20191 and 20196. Reproducible and appropriate positions are achieved by means of the in-house phantom illustrated in Fig.3[57].

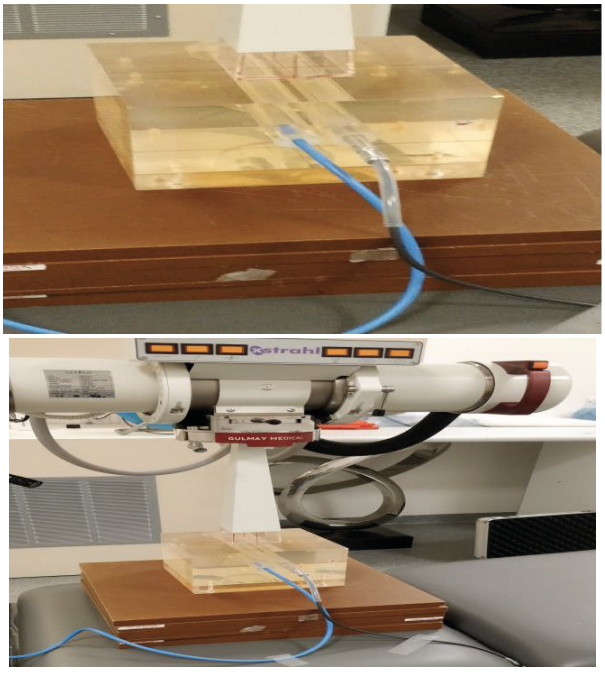

***Fig.3**. Set-up for the inter-comparison work with the chambers inside the Perspex block inserts at 5cm of depth, and minimizing the heel effect. An square 6cm applicator (FSD=50cm) is selected to reduce the stem irradiation, flushing with the phantom surface.*

The calculation of the absorbed dose in water at the reference depth for HVL=2.04mm-Cu is derived from the IPEM X-rays Code of Practice (CoP)[57]:

$$D_w(z) \propto M \cdot [N_{K,Q_0} \cdot k_{ch,Q_0}] \cdot ACF \qquad (11)$$

where M is the integrated charge, ACF the air density factor, z the depth in phantom (5.0 cm), $N_{K,Q}0$ the specific chamber calibration factor at the quality of the intercomparison Q_0, in grays per scale of reading to convert the instrument reading to air kerma free in air. For the SS, N_K is taken from the certificate and includes the recombination factor. Finally, $k_{ch,Q}0$ is the overall factor that corrects for the combined effect of the change in quality between the in-air and in-phantom scenarios, the displacement due to the wall and air cavity and the chamber stem effect[57]. The previous proportionality turns to equality if the ratio of mass attenuation coefficients and the phantom and distance corrections are included. As these values keep constant in the simultaneous irradiation, then (7) leads to the next calibration coefficient:

$$[N_{K,Q_0}^{cross} \cdot k_{ch,Q_0}]_{PP} = N_{K,SS} \cdot k_{ch,Q_0,SS} \cdot \left(\frac{M_{SS}}{M_{PP}}\right) \quad (12)$$

Referred to SS, the k_{ch} value found in the literature[57,60] for our conditions is near 1.012. Possible deviations from this value will be treated as uncertainties (see Appendix 2).

The inserts will be swapped and the readings repeated (at least 3 exposures) in two set of measurements. The true ratio of the instrument readings is then given by:

$$\left(\frac{M_F}{M_{PP}}\right) = \sqrt{\left(\frac{M_F}{M_{PP}}\right)_{1st} \cdot \left(\frac{M_F}{M_{PP}}\right)_{2nd}} \quad (13)$$

where $\left(\frac{M_F}{M_{PP}}\right)_{1st-2nd}$ is the mean of ratios $\frac{M_F}{M_{PP}}$ for the first and second series. The standard error of the mean of all ratios calculated should normally be less than 1% (0.5% of either series).

An example of this procedure is shown in Appendix 2. These numbers must be updated on an annual basis.

METHODS AND RESULTS FOR BT MEASUREMENTS

The set-up for the measurement of the absorbed-dose in BT is illustrated in Fig.4. For this purpose, a new rectangular block inside the WTE phantom used for electron dosimetry has been built, hosting the detector and the source guide in a reproducible way. The phantom should be placed consistently between water equivalent RMI layers to simulate a complete scattering medium. After the characterization of the backscatering effect illustrated in Fig.5, 8.0cm were decided to be placed above. The contribution of the inferior layers is minor, though for consistency purposes, 4.0cm are proposed. Given that the distance source-detector is nearly 4.75cm, an accurate source and detector positioning are required and satisfied with both inserts.

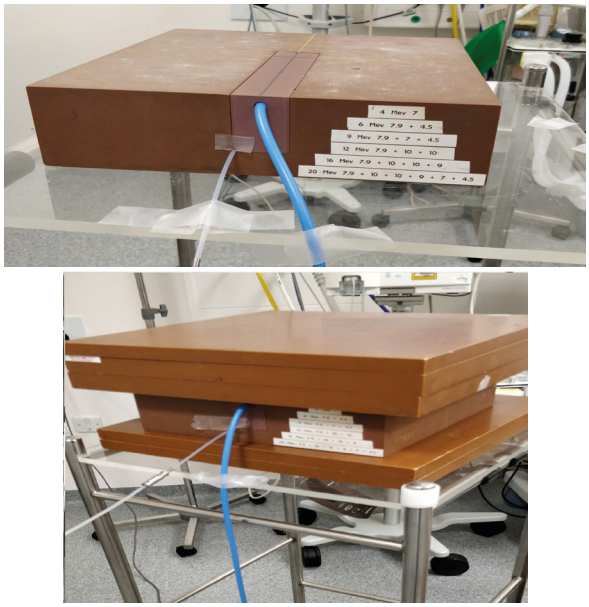

Fig.4*. Set-up for the measurements of the absorbed dose by the chamber. A plastic flexible applicator of diameter 2.8mm is connected to the source guide and inserted into the new WTe rectangular block. The phantom is sandwiched consistently by solid water layers.*

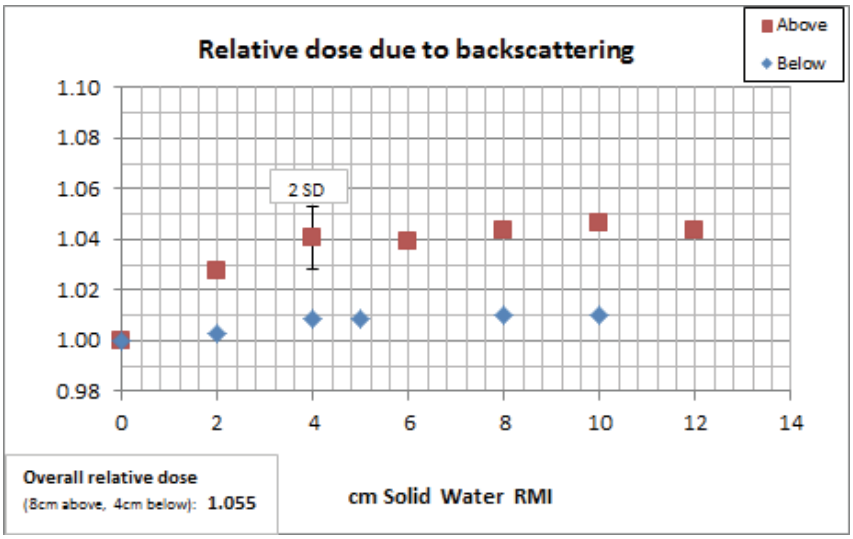

***Fig.5**. Quantification of the backscattering effect. The overall relative overdosage is 5.5% (4.5+1.0), with the contribution of the above layers near to 4.5%. This study justifies the importance of placing consistently the solid water layers.*

Source 38 (ACF=1.019)	**Source 39** (ACF=1.008)	**Source 40** (ACF=1.008)	**Source 40** (ACF=1.023)	**Source 41** (ACF=1.033)	**Source 41** (ACF=1.019)	**Source 41** (ACF=1.019)	**Source 41** (ACF=1.019)
101.4 ± 4.2	100.9 ± 4.2	101.1 ± 4.2	101.3 ± 4.2	100.4 ± 4.1	104.4 ± 4.3	103.9 ± 4.3	104.1 ± 4.3

Table 2: Measurement of the absorbed dose (cGy) for different HDR sources [± 2SD]

Source 38	**Source 39**	**Source 40**	**Source 40**	**Source 41**	**Source 41**	**Source 41**	**Source 41**	**Mean Diff.**	**Std.Dev. in the Diff. (k=1)**
100.5 (-0.9 %)	100.5 (-0.4 %)	100.5 (-0.6 %)	100.5 (-1.0 %)	100.5 (0.1 %)	100.5 (-3.7 %)	100.5 (-3.2 %)	100.5 (-3.4 %)	-1.6 %	1.5

Table 3: MC doses (cGy) and differences w.r.t. experience (%)

Source 38	**Source 39**	**Source 40**	**Source 40**	**Source 41**	**Source 41**	**Source 41**	**Source 41**	**Mean Diff.**	**Std.Dev. in the Diff. (k=1)**
99.94 (-1.4 %)	99.94 (-0.9 %)	99.94 (-1.1 %)	99.94 (-1.5 %)	99.94 (-0.4 %)	99.94 (-4.2 %)	99.94 (-3.7 %)	99.94 (-3.9 %)	-2.2 %	1.5

Table 4: TPS doses (cGy) and differences w.r.t. experience (%)

A reference plan has been created in 'Eclipse Brachytherapy' using a specific phantom CT scan, and then delivered for different HDR sources along the last 2 years. The plans consisted of a single line applicator, with 8 dwell positions. The normalization has been done so that the dose at the effective point of the chamber is 100cGy.

Per measurement, the charge is collected and then corrected by the factors of expressions (2)&(3). The data are recorded electronically in a program coded in Visual Basic 2010 that has been built. This software enables the user to add, delete and compare the results with the expected values within a data-table (example given in Appendix3). The absorbed doses are presented in Table 2 and their uncertainties are evaluated in the Appendix 2.

VERIFICATION OF RESULTS

COMPARISON WITH MONTE CARLO CALCULATIONS

The dose estimation in the effective point of measurement has been performed by MC calculations and compared with the previous results. For an exhaustive detail of this procedure, refer to Appendix 4.

This estimation is based on TG-43U formalism under the away-along coordinates and pre-calculated DRT (dose rate per unit of source strength) values by the general purpose code GEANT4.

Multiplying the DRTs by the respective unit of source strength and dwell time, the dose delivered by a source position is obtained. Adding linearly the contributions of each dwell source, $D_{w,i}$, and disregarding the transit dose effect -negligible in this geometry[73]- the total absorbed dose is:

$$D_w = \sum_i D_{w,i} \qquad (14)$$

Specifically for our geometry, the final estimation of dose and their differences with regards to our measurements (MC-Measurement) are presented in Table 3:

COMPARISON WITH ECLIPSE BRACHYTHERAPY TREATMENT PLANNING SYSTEM

The estimation by the TPS is done in the Eclipse plan *ID:170518*. The reference point created 'Effective Point' represents the effective point of measurement with a normalization of 100 cGy per fraction. The dose at this point and differences with regards to the measurements (TPS-Measurement) are shown in Table 4:

DISCUSSION

Overall, the results presented in Table 3 and Table 4 show a satisfactory agreement between the dose measure- ments and expected values by independent theoretical estimations. The discrepancy in the mean differences is less than 3%, what is a tight tolerance in this field given the existing limitations in the empirical BT dosimetry and TPS dose calculation engines nowadays.

The **transit dose** effect -a current limitation on BT due to the interdwell, entrance and exit source movement along the catheter- is typically disregarded by most BT planning systems. Actually, with the proposed method following 1d-geometries, this effect can be studied and roughly quantified for a specific source strength. As a con- sequence of this study, it can be claimed that this effect for single channel applicators is **negligible**.

The **AAPM TG-43** dose calculation formalism has provided BT community with clear processes in terms of source strength specification and efficient dose calculations that made it easier to compare dose-outcome rela- tionships among different institutions. It is important to acknowledge that the **bulk of clinical BT dosimetry experience** is with radiation transport and energy deposition in water, with dose to water reported (as calculated under the TG-43 approach). Nevertheless, as it is reviewed by *Rivard et al in Medical Physics Vision 20/20 article (2009)*, the accepted clinical dose parameters can be over-or under-estimated by at least 5 % (and by as much as factor of 10) in numerous situations. This is due to the limitations of the TPS formalism applied to each technique in question, generally the influence of tissue and applicator heterogeneity as well as the finite patient dimensions.

In contrast, model-based dose-calculation algorithms (MBDCAs) offer the possibility of departing from water- only geometries by modelling radiation transport in non-water media (tissues, applicators, air-tissue interfaces), resulting in a much more physically accurate reconstruction of the dose distribution delivered in the patient (as it is discussed in the **TG-186** report[85]). In this sense, this study offers potentially a **compromise** between the codes of practice developed in the protocols TG-43 and TG-186. As a future tool, the limitations of the TPS based on the current TG-43 dosimetry may be quantified. Hence, for the time being the recommendation that TG-43 calculations be performed in parallel with model-based dose calculations is crucial. Only in this way will the radiation therapy community become familiar with dose differences, including the impact on prescription dose and doses to points, organs, and regions of interest. This will enable assessment of the implications of adopting MBDCAs for treatment planning, and help the BT community to understand new study results and place them in the context of previous dose calculations, treatment planning, and research. To ease the department work, the ocial documentation has been attached to the main Electronic QA software by means of independent modules.

COMPARISON TO OTHER DETECTORS IN BT DOSIMETRY

The expanded uncertainty estimated in the Appendix 2 of this report to measure the absorbed dose by our micro-ionization chamber has been **4.1% (k=2)**.

TLDs have been the main dosimeter used for measurement of BT source dose. Typically, these measurements have been made in solid--water phantoms comprised of plastics having radiological characteristics similar to wa- ter. If care is taken, an overall estimate of the expanded uncertainty for the absorbed dose would be: **5.6% (k=2)**[77].

Radiochromic film has also become a common detector for BT measurements. In general, the handling of the film can be important so that exposure to ultraviolet light and other conditions are minimized; again the uncertainty can be reduced if this care is taken. An estimate of the expanded uncertainty is: **10.0 % (k=2)**[78,79].

Occasionally, measurements in a water phantom use **diode or diamond** detectors, but their dosimetric un- certainties can exceed 15% (k=1) for low-energy photon-emitting BT sources[81]. These uncertainties result from the large energy dependence of its absorbed--dose sensitivity, non-linearity, directional dependence, temperature dependence, and bias dependence, especially when used for low-energy BT sources. Diode characteristics are given in the AAPM TG-62 report[82]. **MOSFET** dose response is also energy and dose-rate dependent[81,82]. Whereas MOSFETs have been used for BT in vivo dosimetry[83,84], they have not been used to date for direct BT dosimetry.

CONCLUSIONS

Treatment planning and dosimetry in BT have not developed at the same pace as that of EBRT. There have been many difficulties to carry out an experimental dosimetry that in general cause higher uncertainties in this radiotherapy field. Even so in this context, new limits and procedures for an empirical determination must be designed and improved, since **BT plays an important role** in the curative management of cancers in a wide variety of disease sites, most prominently, gynecological malignancies, breast and prostate cancer.

In particular, this work provides a promising framework for a shift from indirect ^{192}Ir dosimetry to a **direct determination of the absorbed dose to water** for BT sources, which is a more accurate and realistic scenario for the verification of HDR BT treatment planning dose distribution. The measurement

APPENDIX 1. CROSS-CALIBRATION RESULTS FOLLOWING THE IPEMB CoP

(Issue Number: 5.1)

RADIOTHERAPY PHYSICS

Results Record

Kilovoltage Photons (new Code of Practice) - HVL 0.5 to 4.0 mm Cu

Unit:	Gulmay
kV:	250
Q_0 HVL (mmCu)	2.04

Machine Information and Factors

k:	1.000

Secondary Standard Factors from NPL Certificate of Calibration

Applicator 6x6 cm^2

Combination	BT Unidos-PP	(300V) High nC
	Sec.Standard NPL (NE2611A)	(-200V) Med

Digital Dial Non-linearity	1.000
Range Correction	1.000
Charge Calibration (C.div^{-1}):	1.00E-09
Gy to cGy factor	100
$k_{Q,SS,Co}$	1.012

RSS (nc) RPP (div)

Intercomparison Data

Meter / Chamber	Position	RSS	RSS' κ	RPP	(RSS' κ) / RPP	Mean A	Mean B	Mean A + B
BT Unidos-PP	A	4.5270	4.527	172.0		0.0263	0.02787	0.02717
BT Unidos-PP	A	4.5270	4.527	172.0	0.02632			
BT Unidos-PP	A	4.5310	4.531	172.5	0.02627	Std. Err. A	Std. Err. B	Std. Err. A + B
BT Unidos-PP	B	4.6370	4.637	166.5	0.02785	0.00002	0.00001	0.0003
BT Unidos-PP	B	4.6420	4.642	166.5	0.02788			
BT Unidos-PP	B	4.6360	4.636	166.5	0.02784	Std. Err. A %	Std. Err. B %	Std. Err A+B %
BT Unidos-PP	A	4.5250	4.525	171.5	0.02638	0.08	0.03	1.20
BT Unidos-PP	A	4.5200	4.520	171.5	0.02636			
BT Unidos-PP	A	4.5260	4.526	171.5	0.02639	Overall Mean of (RSS' κ) / Rf		
BT Unidos-PP	B	4.6380	4.638	166.5	0.02786	0.02709		
BT Unidos-PP	B	4.6430	4.643	166.5	0.02789			
BT Unidos-PP	B	4.6440	4.644	166.5	0.02789			

Calibration Factor Calculation	
180KV (2mmCu)	9.1000E+07
280KV (4mmCu)	9.1400E+07

Field Calibration Factor (cGy.div^{-1})

0.24957

1 div=1pC for BT UNIDOS

Calibration Factor (Gy.C^{-1}):	9.1018E+07
(interpolation curve)	

$$\left[N_{K,Q_0}^{cross} \cdot k_{Q,Q_0}\right] = N_{K,SS} \cdot k_{Q,SS,Q_0} \cdot \left(\frac{M_{SS}}{M_{PP}}\right)$$

Cal. Certificate

kV	mmCu	ln mmCu	Gy/C (to multiply by 10^7)
50	0.03	-3.506557897	9.21
70	0.062	-2.780620894	9.03
100	0.15	-1.897119985	9.02
105	0.2	-1.609437912	9.03
135	0.5	-0.693147181	9.08
180	1	0	9.1
220	2	0.693147181	9.1
280	4	1.386294361	9.14
	2.04	0.712949808	9101840307255

of this magnitude is a progressive and forward-thinking step, presenting illustrative results for the development of BT dosimetry.

The dose formalism described in this paper by using a **cross-calibrated micro-ionization chamber** is novel and was not found elsewhere in literature, accounting on the advantages of using a dosimeter of this nature. Like- wise, it involves a more realistic uncertainty estimation for absorbed dose to water determination compared to the dose-to-water determination based on air-kerma strength in the TG-43 protocol.

Furthermore, an optimized procedure in the quality assurance of the HDR unit at this centre has been established. For this purpose, a new program coded in Visual Basic 2010 has been built. Due to the simple but accurate assem- bly, this methodology is useful for periodical dose management of ^{192}Ir sources under a dose to water formalism, whilst ensuring both nominal and scaled source dwell times and positions in the TPS. The only extra material required to be built has been an internal jig which is inserted into the WTe Electron Phantom -already available for electron dosimetry. The rest of the equipment is typically found in a standard UK radiotherapy department.

As future goal, the above research in BT can be potentially useful for quantifying the existing limitations of the dose calculations made by the TPS in some techniques in question. In this sense and thinking in eventual department techniques, this study may serve as a valuable tool to quantify the impact of the steep dose gradients in interstitial BT applications such as gynecological and prostate treatments.

APPENDIX 2. UNCERTAINTY ANALYSIS

The primary sources of uncertainty in this study are presented in the following table. The uncertainties will be estimated for an above--mentioned measurement regarding a single line applicator to illustrate and simplify calculations. The final expanded percentage is applicable to other report results.

Sources of Uncertainty (x_i)
Cross-calibration coefficient
Perturbation factor
Recombination factor
Polarity factor
Phantom factor
Atmospheric Correction Factor
Collected charge
Source position
Other coefficients in DCF

Assuming independent components x_i, the total uncertainty in the dose, $u_c(D_w)$, is estimated by the quadratic propagation of variance:

$$u_c^2(D_w) = \sum_{i=1} u^2(x_i) \cdot \left(\frac{\partial D_w(x_i)}{\partial x_i} \right)^2 \qquad (15)$$

where $u(x_i)$ represents the the uncertainty associated to any x_i in (2), and $\left(\frac{\partial D_w(x_i)}{\partial x_i} \right)$ is the sensitivity coefficient of x_i.

Each x_i will be evaluated in the next subsections as A-type (evaluation by a statistical analysis of measured quantity values) or B-type (based on scientific judgment using all of the relevant information available).

The measure of uncertainty intended to meet the requirement of expressing the result with a level of confidence is termed expanded uncertainty, $U(D_w)$, and it is obtained by multiplying $u_c(D_w)$ by a coverage factor k:

$$U(D_w) = u_c(D_w) \cdot k \qquad (16)$$

Typically k=2[74], providing approximately a 95% confidence interval.

Uncertainty in the cross-calibration and overall perturbation factor ($N^{cross}_{K,Q} \cdot k_{ch,Q}$)

The calibration coefficient is calculated according to Section 5 of this report:

$$[N^{cross}_{K,Q} \cdot k_{ch,Q}] = [N^{cross}_{K,Q_0} \cdot k_{ch,Q_0}] \cdot k_{Q,Q_0} \cdot k_V \cdot k_{\alpha,p} \quad (17)$$

$$[N^{cross}_{K,Q_0} \cdot k_{ch,Q_0}]_{PP} = \left(\frac{M_{SS}}{M_{PP}}\right) \cdot N_{K,SS} \cdot k_{ch,Q_0,SS} \quad (18)$$

Applying quadratic propagation in the expressions (17) and (18), the overall relative uncertainty is estimated by means of:

$$\epsilon(N^{cross}_{K,Q} \cdot k_{ch,Q}) = \sqrt{\epsilon^2\left(\frac{M_{SS}}{M_{PP}}\right) + \epsilon^2(N_{K,SS}) + \epsilon^2(k_{ch,Q_0,SS} + \epsilon^2(k_{\alpha p}) + \epsilon^2(k_{Q,Q_0}) + \epsilon^2(k_V)} \quad (19)$$

The previous components will be quantified below:

- **A-Components**: The statistical fluctuations in the ratio of collected charges are taken with 1 Standard Deviation (SD) of the geometrical mean within the inter-comparison results. For our example with BT UNIDOS: $(M_{SS}/M_{PP}) = 0.0271 \pm 0.0003$ (0.6%, $k = 1$).
- **B-Components:**
  - The uncertainty in $N_{K,SS}$ is inferred from the NPL certificate of calibration: $N_{K,SS} = (9.1018 \pm 0.055) \cdot 10$ *Gy/nC*, $k = 1$ (0.6%).
  - The value and uncertainty in the overall perturbation factor involved in the cross-calibration can be deducted from some references for our conditions[60]:

$$k^{20cm^2}_{ch,Q_0} = 1.010 \pm 0.008 \ (k = 1) \ \text{[NE2571]} \ ;$$
$$k^{50cm^2}_{ch,Q_0} = 1.014 \pm 0.008 \ (k = 1) \ \text{[NE2571]}.$$

After interpolating the previous values for our applicator size (6x6cm^2) and propagating quadratically the variances:

$$k_{ch,Q_0} = 1.012 \pm 0.013 \quad (k = 1) \ \text{[NE2571]}.$$

The pass from the chamber NE2571 to NE2611(SS) is performed according to IPEMB CoP(p.2617) by adding quadratically 1% to the previous uncertainty:

$$k_{ch,Q_0,SS} = 1.012 \pm 0.016 \quad (k = 1).$$

- The energy shift factor $k_{Q,Q}0$ is quantified as: $k_{Q,Q0} = 1.0026 \pm 0.0025$ (k=1).
- The factor of displacement k_V is given by *Kondo et al.*[65], with a negligible uncertainty in the MC tables (0.1%).
- The factor k_{ap} would correct the response of the field chamber when changing from surroundings air to one of the phantom material at quality Q, instead of taking the inter-comparison phantom as surround- ing material at Q_0 -as it is done by $k_{ch,Q}0$. Since both media are quite similar, the overall perturbation is not affected and this factor is considered as negligible.

Therefore, adding the A and B-components in (19):

- $\epsilon(N^{cross}_{K,Q} \cdot k_{ch,Q}) = 1.8\%.$
- The sensitive coefficient is then: $\left(\frac{\partial D_w}{\partial [N_{K,Q} \cdot k_{ch,Q}]}\right) = \frac{D_w}{N^{cross}_{K,Q} \cdot k_{ch,Q}}$.

The final values are tabled below:

Uncertainty in $[N^{cross}_{K,Q} \cdot k_{ch,Q}]$	
Term	Example
Sensitivity coefficient (div)	405.368
u (cGy/div)	0.0046
Product (cGy)	1.8528

Uncertainty in the phantom factor

For an **unbounded** water medium, this factor is estimated theoretically by MC simulations[44], correcting the radial distance in water by the density of material and assuming that the angle dependence is insignificant respect the radial one. In our case: $k_{p,h}$=1.00 (1σ<0.1%).

Secondly, a component which corrects for the **boundary** of the medium should be included. Differences between bounded and unbounded medium are considered with the uncertainty of **0.75%**(k=1; for details see Appendix 5).

The sensitive coefficient is then written as: $\left(\frac{\partial D_w}{\partial [k_{p,h}]}\right) = \frac{D_w}{k_{p,h}}$.

Uncertainty in $k_{p,h}$	
Term	Example
Sensitivity coefficient (cGy)	101.417
u	0.0075
Product (cGy)	0.7606

UNCERTAINTY IN ACF

T and P are assumed to be B-type components of uncertainty (A-components are negligible in comparison). At the same time, they depend on the resolution and on the calibration of the thermometer and barometer used in the measurements. Each of these contributions are studied below:

- **Resolution uncertainty**: The uncertainty due to the digital resolution limitation in the pressure readings and to the analogical resolution in the temperature (will depend on the operator) is quantified as follows. If the device resolution is u(x), the value of the input signal that produces a value X is located with the same probability in the interval [X-u(X), X+u(X)]-following a rectangular distribution of probability- having a range of: u(x)=±u(*T, P*)/√3.

The relative standard deviation for ACF is:

$$[u(ACF)/ACF]^2 = [u(T)/T]^2 \cdot \left(\frac{T}{T+273.15}\right)^2 + [u(P)/P]^2 \quad , \qquad (20)$$

where $u_1(P) = \pm 1.0/\sqrt{3} = 0.288$ *mbar*, $u_1(T) = \pm 0.25/\sqrt{3} = 0.144$ ˚C.

- **Calibration uncertainty**: The measurements are made with a barometer and thermometer with traceable calibrations. The certificates or internal comparisons report (k=1): $u_2(P) = 0.02$ *mb* (950_1050 *mb*). $u_2(T) = 0.5$ ˚C (10-50 ˚C).

Each uncertainty contribution is squared and summed to produce the squared relative uncertainty:

$$\sqrt{u_1(P)^2 + u_2(P)^2} = \sqrt{u(P)^2} = u(P) = 0.060\ mbar. \qquad u(T) = 0.520\ ^\circ\text{C}.$$

The sensitive coefficient and definitive uncertainty in ACF are then: $\left(\frac{\partial D_w}{\partial [ACF]}\right) = DCF \cdot M = D_w/ACF$

Uncertainty in ACF	
Term	Example
Sensitivity coefficient (cGy)	99.429
u	0.0018
Product (cGy)	0.1790

Uncertainty in the recombination and polarity factors

Applying quadratic propagation in the equations (4) and (5), the next A-components are obtained:

- $u(k_{pol,j}) = k_{pol,j} \cdot \sqrt{u^2(M_j) \cdot \frac{1}{M_j^2} + \frac{u^2(M_{+,j}) + u^2(M_{-,j})}{(|M_{+,j}| + |M_{-,j}|)^2}}$

$$j = BT, XR\ .$$

$$u(k_{ion}) = k_{ion} \cdot \sqrt{\left(\frac{u(k_{ion,BT})}{k_{ion,BT}}\right)^2 + \left(\frac{u(k_{ion,XR})}{k_{ion,XR}}\right)^2}$$

$$j = BT, XR\ .$$

$$u(k_{ion}) = k_{ion} \cdot \sqrt{\left(\frac{u(k_{ion,BT})}{k_{ion,BT}}\right)^2 + \left(\frac{u(k_{ion,XR})}{k_{ion,XR}}\right)^2}$$

- $\left(\frac{\partial D_w}{\partial [k_j]}\right) = D_w/k_j \quad , \quad j = pol, ion\ ,$

where $u(M) \equiv u(M_-)$, $u(M_+)$, $u(M_2)$ are the uncertainty of the reading when the reference negative voltage is selected, when the polarity is positive, and for the half voltage, respectively. They are taken as the statistical dispersion in the readings during the annual characterization: $u(M_-) = 0.058$; $u(M_+) = 0.493$; $u(M_2) = 0.141$.

Uncertainty in kpol		Uncertainty in kion	
Term	Example	Term	Example
Sensitivity coefficient (cGy)	102.826	Sensitivity coefficient (cGy)	101.236
u	0.0022	u	0.0011
Product (cGy)	0.2262	Product (cGy)	0.1114

Uncertainty in the source positioning

Due to the possible axial source mov√ement within ±1*mm*, the new distance source-detector to be considered is calculated by basic trigonometry: $y' = \sqrt{0.100^2 + 4.750^2} = 4.751$ cm.

Applying the inverse quadratic dependence, the dose would be reduced by the factor: $(4.751/4.750)^{-2}$=0.9996. Therefore, this component is less than 0.1% (k=2), and will be regarded as **negligible**.

Uncertainty in the rest of terms

- $\left(\frac{\mu^{en}}{\rho}\right)_{\alpha}^{w}$: According to *Andreo et al.*[75] the estimated MC value is: (1.1110 ± 0.0055) $\lceil k = 1 \rceil$. And the sensitivity coefficient: $\left(\frac{\partial D_w}{\partial\left(\frac{\mu^{en}}{\rho}\right)_{\alpha}^{w}}\right) = D_w/1.111$.

Uncertainty in the relative mass absorption coefficient	
Term	Example
Sensitivity coefficient (cGy)	91.2824
u	0.0055
Product (cGy)	0.5021

- **$(1\text{-}g_{\alpha})$:** Values are referenced in DIN 6814-3 , with **insignificant** uncertainties.

Combined uncertainty

The total uncertainty in D_w is calculated using (11), (12) and k=2:

Expanded total uncertainty U_c
4.2 cGy (4.1%)

APPENDIX 3. DOSE MEASUREMENT EXAMPLE IN THE NEW EXECUTABLE

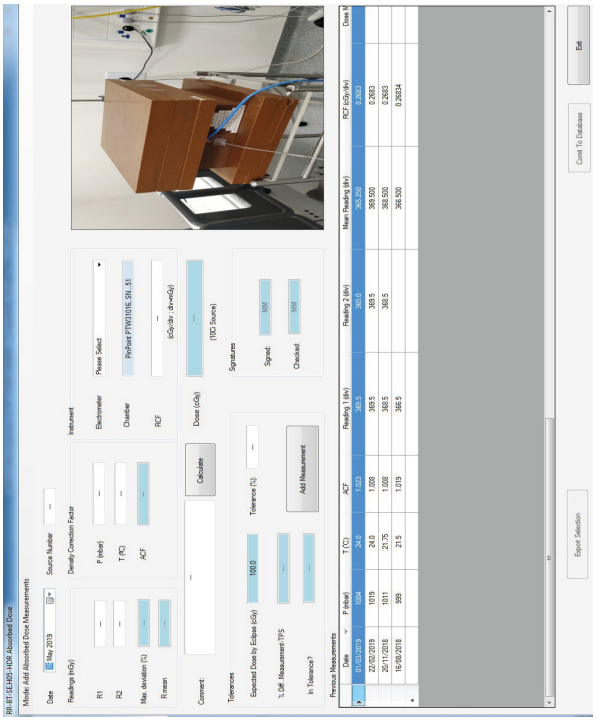

APPENDIX 4. MC CALCULATIONS FOR THE HDR SOURCE

The mechanical design of the ^{192}Ir source at the local centre is shown in Fig.6. The active core consists of a cylinder with a diameter of 0.06cm and length 0.35cm, made of iridium metal. There are different encapsulation geometries resulting in an outer diameter of 0.11 and 0.09cm for the 12i and Plus model, respectively.

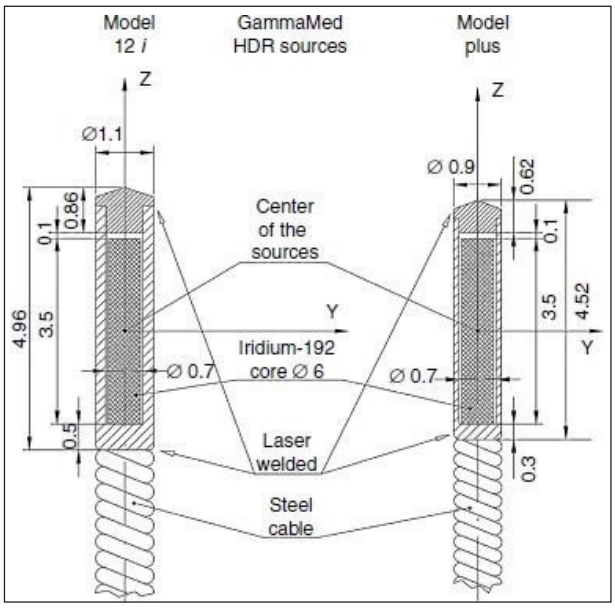

***Fig.6**. GammaMed HDR ^{192}Ir source type geometrical designs for the GammaMed 12i and Plus afterloaders.*

Dose Rate Look-Up Tables

The primary information used for deriving the TG-43/TG-43 U1 data is a dose rate table per unit source strength, DRT, which is usually expressed in cGy $h^{-1}U^{-1}$. This is a "dissemble-and-assemble" factorization approach[80]; first derive from the DRT the TG-43 U1 parameters, and then apply these utilizing the following expression on to calculate the dose rate value at the required place:

$$D(r,\theta) = \Lambda \frac{G_L(r,\theta)}{G_L(r_0,\theta_0)} \cdot g_L(r) \cdot Fr,\theta) \quad , \ (21)$$

where Λ is the dose rate constant (defined as the dose rate to water in water at the reference point, namely at a distance of r_0=1cm on the transverse axis- $\theta_0=\pi/2$), per unit of kerma strength, S_K, depending on the radionuclide and source model, and on the methodology used to determine S_K; $G_L(r, \theta)$ is the geometry function at a radial distance r and polar angle θ as a dimensionless quantity that establishes the effective inverse square-law correction based upon the spatial distribution of radioactivity within the core; $g_L(r)$ is the radial dose function that considers the distance dependence of absorption and scatter of the photon rays in the water medium along the transverse axis(y-axis) as a dimensionless quantity; F(r,θ)the anisotropy function that considers the effect of absorption and scatter of the photons within the source active core and encapsulation material as well as part of the driving cable, as a dimensionless quantity too.

Although from a practical point of view DRTs could be much more useful if they are expressed as radial distance r and polar angle θ, dose rate tables (in polar coordinates), commonly published DRTs, are expressed as along-away tables (Cartesian coordinates). Along means the z and away the y-axis of the TG43 coordinate shown in the previous image. This is due to the fact that using polar coordinates a higher resolution at short distances can be achieved in accordance to the variation of the dose rate gradient around the sources.

While extrapolations outside an existing DRT can be easily handled (similarly to TG-43 parameters), the accuracy of interpolation between DRT values is questionable. Despite the physical content/meaning of the geometry function $G_L(r)$, this can be utilized to filter out, to a very high degree, the large dose rate gradients existing when moving along a ray, at a specific polar angle θ or moving along an arc, for a specific radial distance r. The same is valid when an along-away table is considered, and a bilinear interpolation has to be applied along the y and z-axis. In this way the accuracy of the bilinear interpolation is significantly improved.

In Fig.7 this effect is graphically demonstrated for the example of the new microSelectron HDR ^{192}Ir source.

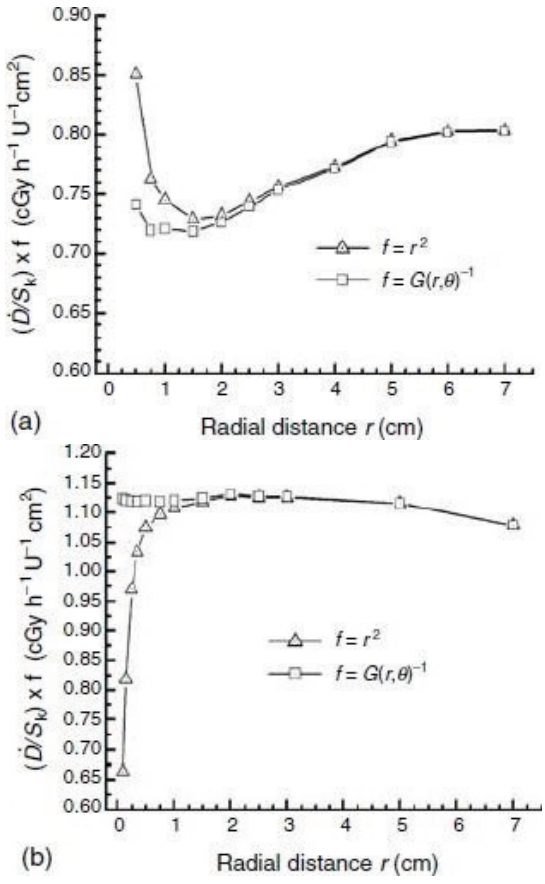

Fig.7*. Demonstrating of improving interpolation accuracy when using dose rate look-up tables(LUTs) instead of analytic expressions such us TG43U dosimetry protocol.The dose rate per unit of source strength table values for the microSelectron HDR source design have been multiplied by the factor f, which is the inverse of the corresponding geometry function value either for the point source approximation or the line source approximation for polar angle 0 (a) or π/2 (b). The homogenization effect when applying the line source approximation of the geometry function based factor f is clearly demonstrated, thus resulting in very accurate results when performing interpolations among tabulated values (LUT).*

Look-up tables (LUT) in Cartesian (along--away) or polar coordinates (r, θ) of dose rate per unit source length multiplied by the corresponding geometry function value obtained using the line source approximation could be used either for computations or for verifications:

$$LUT(y,z) = \frac{D(y,z)}{S_K} \cdot \frac{1}{G_L(y,z)}$$

$$[cGyh^{-1}U^{-1}cm^2] \quad , \qquad (22)$$

where:

$$G_L(r,\theta) = \frac{\beta}{L_s \cdot r \cdot sin(\theta)} \quad , \qquad (23)$$

with $r=+\sqrt{y^2+z^2}$, $\theta = atan(y/z)$, L_s and β defined in Fig.8.

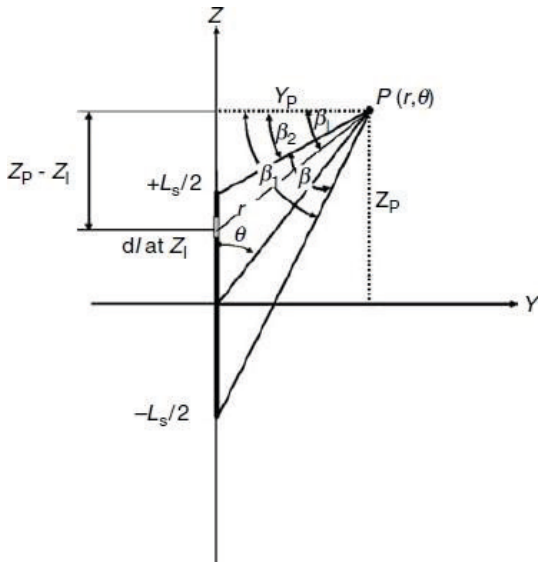

Fig.8*. Parameters used for deriving analytical expression of the geometry function for the line source approximation.*

After the interpolation among LUT values, the final value has to be multiplied by the corresponding geometry function value to obtain the dose rate per unit source strength at the point of interest. This methodology, using LUTs, simplifies the data handling and also enables the handling of new source types such as miniaturized x-rays sources or cylindrical asymmetric designs where 3d LUT can be easily considered.

DOI https://doi.org/10.22533/at.ed.317522503024

EXPECTED DOSES @ THE EFFECTIVE POINT BY MONTE CARLO

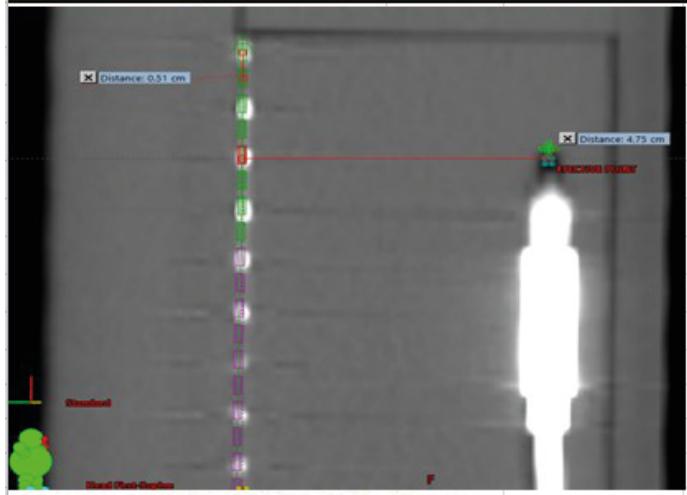

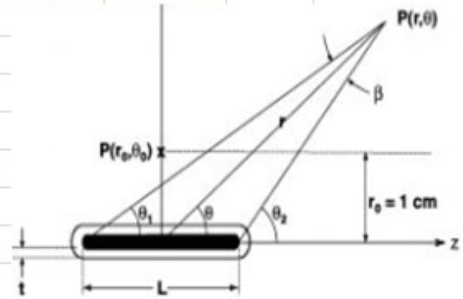

Coordinate system used for brachytherapy dosimetry calculations.

(coordinates away and along in TG-43 geometry)

(Source: GammaMed HDR Ir192 Model Plus Design)

z4 (cm) (positive if we are in the sense of the tip)	0.0	**DRT (cGy/h/U)**	**0.049891**				
y (cm) (fixed coordinate)	**4.75**	**distance source-effective point measurement (cm) :**				4.75	
z5(cm)	0.50	**DRT (cGy/h/U)**	**0.049444**	**z3(cm)**	-0.5	**DRT (cGy/h/U)**	**0.049376**
z6 (cm)	1.0	**DRT (cGy/h/U)**	**0.047727**	**z2 (cm)**	-1.0	**DRT (cGy/h/U)**	**0.047865**
z7(cm)	1.5	**DRT (cGy/h/U)**	**0.045213**	**z1 (cm)**	-1.5	**DRT (cGy/h/U)**	**0.045332**
z8 (cm)	2.0	**DRT (cGy/h/U)**	**0.042137**	(values not exactly symmetrical in Z, but almost.)			

(DRT values where Drate per unit of strength is shown: Table A.4.7.Baltas)

dwell time for all positions (h)	**0.015361111**	(23.6s 10Ci source)
$T_{1/2}$**(days)**	73.83	*(IN GREEN TO UPDATE IN EACH SOURCE)*
Issued Air kerma rate (cGy/h)	**4.967**	
Day of reference	**26/04/2018**	
Distance of reference (cm)	100	
Day of measurement	**16/08/2018**	
t elapsed from reference (days) :	112	
RAKR at day of measurementand at 1m (cGy/h)	1.7355	
Strenght at day of measurement (U)	17355.2992	
Dw @ the effective point (cGy)	**100.50**	

DOI https://doi.org/10.22533/at.ed.317522503024

EXAMPLE INTERPOLATION IN LUT AND THEN PASSING TO DRT FOR THE 3RD MEASUREMENT IN A SINGLE SOURCE POSITION

(All distances in cm and angles in radians)

DRT	0.0311	DRT	0.0451	**AFTER**	
z	0.0	z	0.0	z	0.0
y	6.0	y	5.0	y	5.14
ls	0.35	ls	0.35	ls	0.35
pi	3.141592654	pi	3.141592654	pi	3.1415927
theta2	1.599954727	theta2	1.605782046	theta2	1.6048299
theta1	1.541637927	theta1	1.535810608	theta1	1.5367628
alfa2	1.541637927	alfa2	1.535810608	alfa2	1.5367628
alfa1	0.0291584	alfa1	0.034985719	alfa1	0.0340335
beta	0.0583168	beta	0.069971438	beta	0.0680671
G	0.027769905	G	0.039983679	G	0.0378361
LUT	1.119917407	LUT	1.127960246		

LUT interpolated	**1.126834248**
DRT after interpolated LUT	**0.04263498**

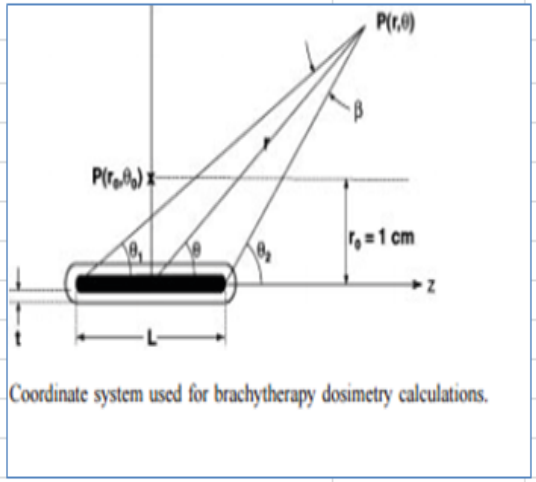

Coordinate system used for brachytherapy dosimetry calculations.

$$G_P(r,\theta) = r^{-2} \quad \text{point-source approximation,}$$

$$G_L(r,\theta) = \begin{cases} \dfrac{\beta}{Lr\sin\theta} & \text{if} \quad \theta \neq 0° \\ (r^2 - L^2/4)^{-1} & \text{if} \quad \theta = 0° \end{cases} \qquad \text{line-source approximation,}$$

TABLE A.4.7

Monte Carlo (MC) Calculated Dose Rate Values Per Unit Source Strength as an Along–Away Dose Rate Table (DRT) for the GammaMed HDR ^{192}Ir Source *Model Plus* Design

Distance Along	Dose Rate Per Unit Source Strength (cGy $h^{-1} U^{-1}$) Distance Away y (cm)																	
z (cm)	0.03	0.20	0.40	0.60	0.80	1.00	1.25	1.50	1.75	2.00	2.50	3.00	3.50	4.00	5.00	6.00	8.00	10.00
10.00	0.00836	0.00834	0.00841	0.00848	0.00848	0.00856	0.00854	0.00857	0.00860	0.00860	0.00857	0.00849	0.00834	0.00814	0.00765	0.00707	0.00580	0.00464
8.00	0.0129	0.0131	0.0131	0.0132	0.0134	0.0135	0.0136	0.0137	0.0137	0.0137	0.0136	0.0133	0.0129	0.0124	0.0113	0.0101	0.00779	0.00591
6.00	0.0225	0.0227	0.0233	0.0236	0.0239	0.0243	0.0245	0.0247	0.0246	0.0245	0.0237	0.0227	0.0214	0.0201	0.0173	0.0146	0.0104	0.00741
5.00	0.0321	0.0325	0.0335	0.0341	0.0347	0.0352	0.0354	0.0354	0.0351	0.0346	0.0329	0.0308	0.0284	0.0260	0.0215	0.0176	0.0118	0.00818
4.00	0.0488	0.0497	0.0517	0.0533	0.0540	0.0550	0.0550	0.0543	0.0531	0.0515	0.0473	0.0429	0.0383	0.0340	0.0267	0.0209	0.0134	0.00892
3.50	0.0623	0.0643	0.0673	0.0699	0.0712	0.0717	0.0712	0.0695	0.0671	0.0643	0.0577	0.0510	0.0446	0.0389	0.0296	0.0227	0.0141	0.00927
3.00	0.0837	0.0867	0.0919	0.0952	0.0969	0.0970	0.0950	0.0914	0.0875	0.0818	0.0711	0.0610	0.0519	0.0443	0.0326	0.0245	0.0148	0.00956
2.50	0.119	0.125	0.133	0.138	0.139	0.138	0.131	0.124	0.115	0.105	0.0878	0.0727	0.0601	0.0501	0.0357	0.0262	0.0154	0.00986
2.00	0.181	0.197	0.211	0.216	0.214	0.204	0.189	0.172	0.154	0.137	0.108	0.0859	0.0689	0.0560	0.0386	0.0278	0.0160	0.0101
1.75	0.235	0.260	0.279	0.283	0.273	0.258	0.231	0.204	0.179	0.156	0.120	0.0931	0.0735	0.0590	0.0400	0.0285	0.0162	0.0102
1.50	0.322	0.356	0.382	0.379	0.357	0.326	0.284	0.244	0.208	0.178	0.132	0.100	0.0777	0.0617	0.0412	0.0292	0.0165	0.0103
1.25	0.454	0.526	0.553	0.528	0.478	0.420	0.350	0.290	0.241	0.201	0.144	0.107	0.0817	0.0642	0.0423	0.0297	0.0167	0.0104
1.00	0.716	0.845	0.861	0.773	0.656	0.546	0.432	0.343	0.276	0.225	0.156	0.113	0.0854	0.0665	0.0433	0.0302	0.0168	0.0104
0.80	1.19	1.37	1.30	1.08	0.854	0.674	0.506	0.387	0.304	0.243	0.164	0.118	0.0879	0.0681	0.0440	0.0306	0.0169	0.0105
0.60	2.23	2.52	2.10	1.53	1.11	0.818	0.583	0.431	0.330	0.259	0.172	0.121	0.0900	0.0693	0.0445	0.0308	0.0170	0.0105
0.40	6.05	5.68	3.51	2.14	1.39	0.963	0.652	0.467	0.351	0.272	0.177	0.124	0.0915	0.0702	0.0449	0.0310	0.0170	0.0106
0.20	—	15.0	5.50	2.76	1.64	1.08	0.702	0.493	0.365	0.280	0.180	0.126	0.0923	0.0707	0.0451	0.0311	0.0171	0.0106
0.00	—	23.2	6.63	3.05	1.73	**1.118**	0.720	0.501	0.370	0.283	0.182	0.126	0.0926	0.0709	0.0451	0.0311	0.0171	0.0106
−0.20	—	15.1	5.50	2.77	1.64	1.08	0.701	0.493	0.365	0.280	0.180	0.126	0.0923	0.0707	0.0451	0.0311	0.0171	0.0105
−0.40	—	5.70	3.51	2.15	1.40	0.965	0.652	0.468	0.351	0.272	0.177	0.124	0.0913	0.0701	0.0448	0.0310	0.0170	0.0105
−0.60	—	2.52	2.09	1.53	1.11	0.820	0.582	0.431	0.330	0.259	0.171	0.121	0.0899	0.0693	0.0445	0.0308	0.0170	0.0105
−0.80	—	1.36	1.30	1.08	0.857	0.676	0.506	0.388	0.304	0.243	0.164	0.118	0.0878	0.0681	0.0440	0.0306	0.0169	0.0105
−1.00	—	0.833	0.858	0.776	0.659	0.549	0.431	0.343	0.276	0.225	0.156	0.113	0.0853	0.0665	0.0434	0.0302	0.0168	0.0104
−1.25	—	0.512	0.552	0.531	0.481	0.421	0.350	0.290	0.241	0.201	0.144	0.107	0.0817	0.0643	0.0424	0.0298	0.0166	0.0104
−1.50	—	0.343	0.381	0.380	0.359	0.328	0.284	0.244	0.208	0.178	0.132	0.1001	0.0776	0.0618	0.0413	0.0292	0.0164	0.0103

(continued)

Journal of Engineering Research ISSN 2764-1317

DOI https://doi.org/10.22533/at.ed.317522503024

DOI https://doi.org/10.22533/at.ed.317522503024

—*Continued*

Distance Along	Dose Rate Per Unit Source Strength (cGy h^{-1} U^{-1}) Distance Away y (cm)																
z (cm)	0.03	0.20	0.40	0.60	0.80	1.00	1.25	1.50	1.75	2.00	2.50	3.00	3.50	4.00	5.00	6.00	8.00	10.00
−1.75	—	0.246	0.276	0.283	0.274	0.257	0.231	0.204	0.179	0.157	0.120	0.0929	0.0733	0.0589	0.0400	0.0285	0.0162	0.0102
−2.00	—	0.184	0.208	0.216	0.214	0.205	0.189	0.171	0.154	0.137	0.108	0.0859	0.0689	0.0561	0.0386	0.0278	0.0160	0.0101
−2.50	—	0.114	0.130	0.137	0.139	0.137	0.132	0.123	0.115	0.106	0.0879	0.0726	0.0601	0.0501	0.0356	0.0262	0.0154	0.00985
−3.00	—	0.0772	0.0885	0.0941	0.0965	0.0970	0.0953	0.0915	0.0869	0.0820	0.0710	0.0608	0.0518	0.0442	0.0326	0.0245	0.0148	0.00958
−3.50	—	0.0563	0.0641	0.0685	0.0706	0.0713	0.0711	0.0695	0.0672	0.0645	0.0577	0.0510	0.0446	0.0389	0.0295	0.0227	0.0141	0.00925
−4.00	—	0.0428	0.0488	0.0519	0.0537	0.0546	0.0549	0.0544	0.0531	0.0513	0.0474	0.0428	0.0382	0.0340	0.0266	0.0209	0.0133	0.00891
−5.00	—	0.0269	0.0308	0.0328	0.0340	0.0348	0.0353	0.0354	0.0351	0.0345	0.0329	0.0308	0.0284	0.0260	0.0215	0.0176	0.0118	0.00816
−6.00	—	0.0192	0.0211	0.0225	0.0234	0.0239	0.0243	0.0245	0.0245	0.0243	0.0237	0.0226	0.0215	0.0201	0.0173	0.0146	0.0104	0.00740
−8.00	—	0.0110	0.0120	0.0125	0.0129	0.0133	0.0135	0.0135	0.0136	0.0136	0.0135	0.0133	0.0129	0.0124	0.0113	0.0101	0.00779	0.00591
−10.00	—	0.00706	0.00751	0.00777	0.00802	0.00816	0.00834	0.00842	0.00848	0.00852	0.00855	0.00846	0.00833	0.00814	0.00765	0.00706	0.00581	0.00464

Data not shown correspond to points within the encapsulated source. The dose rate constant, Λ, marked in bold is the dose rate per unit source strength at the reference point, $r = 1.0$ cm and $\theta = 90°$ or in Cartesian coordinates $y = 1.0$ cm and $z = 0.0$ cm.

Source: From Ballester, F., Puchades, V., Lluch, J.L., Serrano-Andrés, M.A., Limami, Y., Pérez-Calatayud, J., and Casal, E., *Med. Phys.*, 28, 2586–2591, 2001.

APPENDIX 5. ESTIMATION OF $k_{p,h}$.

CRUDE MC ESTIMATION

Most of MC tables refer to different phantom materials in **unbounded geometries** -simulated with an ideal point source located at the centre of an external radius of 80.0cm for several radionuclides.

The following interval of values is estimated by MCNP simulations, for a variety of water equivalent phantoms (WTP) and our empirical radial distance -$r_0 = 4.8cm$[4]:

$$k_{p,h}(r)^{unbounded} = (1.000 - 1.015) \quad [2\sigma < 0.1\%]. \quad (24)$$

CORRECTION OF THE BOUNDED GEOMETRY

Firstly, the estimation of the volume of our in-house phantom is done approximately by multiplying the dimensions: V ≈ 30x8 x17.5 =4200 cm^3.

The measurement phantom is considered equivalent, in terms of scattering and absorption effects, to one bounded medium of same volume and material (sphere with radius R=-10cm, V≈ $4200cm^3$), by using a correction factor $(F_{corr})^{70}$:

$$k_{ph}^{bounded}(r_0) = k_{ph}^{unbounded}(r_0) \cdot F_{corr}(r_0) \quad (25)$$

$$F_{corr}(r_0) = \frac{g^{WTE}(r_0)}{g^{water}(r_0)} \quad , \quad (26)$$

where the new factor F_{corr} is estimated by Geant4 as a ratio of radial dose functions defined by TG-43:

$$g^{water}(r_0) \approx 0.965 \ (2\sigma \approx 0.3\%) \quad [water]. \quad (27)$$

$$g^{WTE}(r_0) \approx g^{water}(1.04 * r_0) \approx 0.960 \ (2\sigma \approx 0.3\%)$$

$$[re - scaling\ with\ the\ WTE\ density]. \quad (28)$$

Overall, the phantom factor corrected is obtained by the previous values:

$$k_{ph} = (0.995 - 1.010) \quad [2\sigma \approx 0.3\%].$$

The definitive value in the phantom factor is taken as the previous mean, and the uncertainty, as the difference between the extreme and central value:

$$k_{ph}(r_0) = 1.003 \pm 0.015 \quad [k = 2]. \quad (30)$$

ACKNOWLEDGMENTS

I would like to thank my colleague Ian Seedhouse for the time and effort given in the supervision of this project.

COMPETING INTERESTS

The author has no relevant conflicts of interest to disclose.

> "Nothing in life is to be feared, it is only to be understood. Now is the time to understand more, so that we may fear less".

REFERENCES

[1]. Bidmead, A.M. et al.(IPEM Working Party).The IPEM code of practice for determination of the reference air kerma rate for HDR 192Ir brachytherapy sources based on the NPL air kerma standard.Phys. Med. Biol. 55 (2010).

[2]. Venselaar, J. European Guidelines for Quality Assurance in Radiotherapy, A Practical Guide to Quality Control of Brachytherapy Equipment Booklet No 8, ESTRO, Belgium, 2004.

[3]. Report of AAPM, Task Group No.32. Specification of brachytherapy source strength. June 1987. [4]. Baltas, D. The Physics of Modern Brachytherapy for Oncology. 2007.

[5]. ICRU 58 (Dose and Volume Specification for Reporting Interstitial Therapy), by International Commission on Radi- ation Units and Measurements.Med. Phys. 25, 1225 (1998).

[6]. Nath et al. Dosimetry of interstitial brachytherapy sources: Recommendations of the AAPM Radiation Therapy Committee Task Group 43, Med. Phys., 22,209 – 234, 1995.

[7]. Rivard et al. Update of AAPM Task Group No. 43 Report: A revised AAPM protocol for brachytherapy dose cal- culations, Med. Phys., 31:3, 633 – 674, 2004.

[8]. Daskalov, GM. et al. Monte Carlo-aided dosimetry of a new high dose-rate brachytherapy source. Med Phys 25(11):2200–2208.

[9]. Paiva, G. et al. Brachytherapy dose measurements in heterogeneous tissues.IAEA,April 13 to 16th, 2014. Cusco, Peru.

[10]. Siwek, R.A. et al. Shielding effects of Selectron applicator and pellets on isodose distributions, Radiother. Oncol., 20, 132 – 138,1991.

[11]. Baltas, D. et al. Measurements of the anisotropy of the new Ir-192 source for the microSelectron-HDR, Activity Special Report, No. 3, Nucletron B.V., The Netherlands, 1993.

[12]. Williamson et al. Comparison of calculated and measured heterogeneity correction factors for 125I, 137Cs, and 192Ir brachytherapy sources near localized heterogeneities, Med. Phys., 20, 1993.

[13]. Chiu Tsao, S.T., Anderson, L.L., O'Brien, K., and Sanna, R. Dose rate determination for 125I seeds, Med. Phys., 17, 815 – 825, 1990.

[14]. Luxton, G. et al. Measurement of dose rate from exposure-calibrated 125I seeds, Int. J. Radiat. Oncol. Biol. Phys., 18,1199 – 1207, 1990.

[15]. Nath, R. et al. Dosimetry on the transverse axes of 125I and 192Ir interstitial brachytherapy sources, Med. Phys., 17, 1032 – 1040,1990.

[16]. Sloboda R.S. and Menon, G.V. Experimental determination of the anisotropy function and anisotropy factor for model 6711 I-125 seeds, Med. Phys., 27, 1789 – 1799, 2000.

[17]. Meigooni, A.S. et al. Dosimetric characteristics of the Intersource 103Palladium brachytherapy source, Med. Phys., 27, 1093 – 1100, 2000.

[18]. Meigooni, A.S. et al. Experimental determination of dosimetric characteristics of Bestw 125I brachytherapy source, Med. Phys., 27, 2168 – 2173, 2000.

[19]. Nath, R. and Yue, N. Dosimetric characterization of a newly designed encapsulated interstitial brachytherapy source of iodine-125- model LS-1 Brachyseed TM, Appl. Radiat. Isot., 55, 813 – 821, 2001.496

[20]. Patel, NS. et al. Thermoluminescent dosimetry of the Symmetrae 125I model I25.S06 interstitial brachytherapy seed, Med. Phys., 28, 1761 – 1769, 2001.

[21]. Anagnostopoulos, G. et al. Thermoluminescent dosimetry of the selectSeed 125I interstitial brachytherapy seed, Med. Phys., 29, 709 – 716, 2002.

[22]. Anagnostopoulos, G. et al. In vivo TLD dose verification of transperineal 192Ir HDR brachytherapy using CT-based planning for the treatment of prostate cancer, Int. J. Radiat. Oncol. Biol. Phys., 57, 1183 – 1191,2003.

[23]. Perera, H.et al.Dosimetric characteristics, air-kerma strength calibration and verification of Monte Carlo simulation fore a new 169Yb brachytherapy source, Int. J. Radiat. Oncol. Biol.Phys., 28, 953 – 970, 1994.

[24]. Piermattei, A. et al. P-type silicon detector for brachytherapy dosimetry, Med. Phys., 22, 835 – 839, 1995.

[25]. Fluhs, D. et al. Direct reading measurement of absorbed dose with plastic scintillators—The general concept and applications to ophthalmic plaque dosimetry, Med. Phys., 23, 427 – 434, 1996.

[26]. Williamson, J.F. et al. Plastic scintillator response to low-energy photons, Phys. Med.Biol., 44, 857 – 872, 1999.

[27]. Kirov, A.S. et al. Towards two dimensional brachytherapy dosimetry using plastic scintillator: New highly efficient water equivalent plastic scintillator materials, Med. Phys., 26, 1515 – 1523,1999.

[28]. Rustgi, S.N. Evaluation of the dosimetric characteristics of a diamond detector for photon beam measurements, Med. Phys., 22, 567 – 570, 1995.

[29]. Rustgi, S.N. Application of a diamond detector to brachytherapy dosimetry,Phys. Med. Biol., 43, 2085 – 2094, 1998.

[30]. Nakano, T. et al. High dose-rate brachytherapy source localisation: Positional resolution using a diamond detector, Phys. Med. Biol., 48, 2133 – 2146, 2003.

[31]. Muench, P.J. et al. Photon energy dependence of the sensitivity of radiochromic film and comparison with silver halide film and LiF TLDs used for brachytherapy dosimetry, Med. Phys., 18, 769 – 775, 1991.

[32]. Chiu-Tsao, S.T. et al. High-sensitivity GafChromic film dosimetry for 125I seed, Med. Phys., 21, 651 – 657, 1994. [33]. Hasson, B.F. Chemical dosimetry in the near-zone of brachytherapy sources,Med. Phys., 25, 2076, 1998.

[34]. Dempsey, J.F., Low, D.A., Kirov, A.S., and Williamson, J.F. Quantitative optical densitometry with scanning-laser film digitizers, Med. Phys., 26, 1721 – 1731,1999.

[35]. Bohm, D. et al. Measurements and Monte Carlo, calculations to determine the absolute detector response of ra- diochromic film for brachytherapy dosimetry, Med. Phys., 28, 142 – 146, 2001. Experimental Dosimetry 497

[36]. Farajollahi, A.R. et al. An investigation into the use of polymer gel dosimetry in low dose rate brachytherapy, Br. J. Radiol., 72, 1085 – 1092, 1999.

[37]. Ibbott, G., Maryanski, M., Drogin, A., Gearheart, D., Ranade, M., Painter, T., and Meigooni, A. Characterization of a New Brachytherapy Source by BANGw Gel Dosimetry, in Proceedings of the 1st International Workshop on Radiation Therapy Gel Dosimetry (DosGel '99), pp. 196 – 198, 1999.

[38]. McJury, M. et al. Experimental 3D dosimetry around a high-dose-rate clinical 192Ir source using polyacrylamide gel (PAG) dosimeter, Phys. Med. Biol.,44, 2431 – 2444, 1999.

[39]. Abramson, D. The measurement of three dimensional dose distribution of a ruthenium- 106 ophthalmological appli- cator using magnetic resonance imaging of BANG polymer gels, J. Appl. Clin. Med. Phys., 2, 85 – 89, 2001.

[40]. De Deene, Y.,et al. On the accuracy of monomer/polymer gel dosimetry in the proximity of a high-dose-rate 192Ir source, Phys.Med. Biol., 46, 2801 – 2825, 2001.

[41]. Papagiannis, P. et al. Dosimetry close to an 192Ir HDR source using N-vinylpyrrolidone based polymer gels and magnetic resonance imaging, Med. Phys., 28, 1416 – 1426, 2001.

[42]. Heard et al. Measurement of brachytherapy sources using MAGIC gel, J. Phys.:221–223,2004.

[43]. Pantelis et al. Polymer gel water equivalence and relative energy response with emphasis on low photon energy dosimetry in brachytherapy, Phys. Med. Biol., 49, 3495–3514, 2004.

[44]. Briesmeister, J.F. et al. MCNPTM—A general Monte Carlo N-particle transport code: version 4C Report LA-13709-M, Los Alamos National Laboratory, LosAlamos, N.M., 2000.

[45]. Perera, H. et al. Rapid two-dimensional dose measurement in brachytherapy using plastic scintillator sheet: linear- ity, signal-to-noise ratio, and energy response characteristics.Int. J. Radiat. Oncol. Biol. Phys.,23,1992.

[46]. PTW, Ionization radiation detectors,2016.

[47]. Siwek, R.A. et al. Shielding effects of Selectron applicator and pellets on isodose distributions, Radiother. Oncol., 20, 132 – 138, 1991.

[48]. Waterman, F.M. and Holcomb, D.E. Dose distributions produced by a shielded vaginal cylinder using a high-activity iridium-192 source, Med. Phys., 21,101 – 106, 1994. Experimental Dosimetry 499

[49]. Verellen, D. et al. On the determination of the effective transmission factor for stainless steel avoid shielding and estimation of their shielding efficacy for the clinical use,Med. Phys., 21, 1994.

[50]. Selbach, H.J. and Andrassy, M. Experimentally determined TG-43 data for the BEBIG MultiSource 192Ir HDR source, unpublished data, personal communication,2005.

[51]. Krieger, H. and Baltas, D. Deutsche Gesellschaf fur Medizinische Physik, Praktische Dosimetrie in der HDR-Brachytherapie DGMP-Bericht Nr. 13, 1999.

[52]. British Institute of Radiology and Institute of Physical Sciences in Medicine,Recommendations for Brachytherapy Dosimetry Report of a Joint BIR/IPSM Working Party, BIR, London, 1993.

[53]. Deutsches Institut fur Normung e.V. [DIN] Clinical Dosimetry. Part 2. Brachytherapy with Sealed Gamma Sources, 1993.

[54]. Deutsches Institut fur Normung e.V. [DIN], Procedures of dosimetry with probetype detectors for photon and elec- tron radiation—1997.

[55]. Deutsches Institut fur Normung e.V. [DIN], Clinical dosimetry—Part 5: Application of x-rays with peak voltages between 100 and 400 kV in radiotherapy, 1996.

[56]. International Commission on Radiation Units and Measurements, Dosimetry of High-Energy Photon Beams based on Standards of Absorbed Dose to Water ICRU report 64 (Bethesda: ICRU), 2001.

[57]. The IPEMB code of practice for the determination of absorbed dose for x-rays below 300 kV generating potential (0.035 mm Al-4 mm Cu HVL; 10 – 300 kV generating potential), Phys. Med. Biol., 41, 1996.

[58]. International Atomic Energy Agency, Absorbed dose determination inexternal beam radiotherapy, Technical Reports Series, No. 398, (Vienna: IAEA), 2000.

[59]. Ma, C.M. et al. AAPM protocol for 40–300kV x-ray beam dosimetry inradiotherapy and radiobiology,Med.Phys.28,2001.

[60]. Seuntjens,F. and Verhaegen,F. Dependence of overall correction factor of a cylindrical ionization chamber on field size and depth in mediumenergy xray beams Med.Phys. 23(10), 1996.

[61]. IPEMB, Addendum to the IPEMB code of practice for the determination of absorbed dose for x-rays below 300 kV generating potential (0.035 mm Al- 4 mm Cu HVL), Phys. Med. Biol., 50, 2739–2748, 2005.

[62]. Agostinelli, S. et al. Response to high-energy photons of PTW31014 ion chamber with a central aluminum electrode.

[63]. Attix, H.F. Determination of Aion and Pion in the new AAPM radiotherapy dosimetry protocol, Med. Phys.1984.

[64]. The IPEM code of practice for determination of the reference air kerma rate for HDR 192Ir brachytherapy sources based on the NPL air kerma standard.2010 Phys. Med. Biol. 55 3145

[65]. Kondo, S. and Randolph, M.L. Effect of finite size of ionization chambers on measurement of small photon sources, Rad. Res., 13, 37 – 60, 1960.

[66]. Jan Seuntjens and Frank Verhaegen. Dependence of overall correction factor of a cylindrical ionization chamber on field size and depth in medium energy x-ray beams.

[67]. IAEA TRS-398. Absorbed Dose Determination in External Beam Radiotherapy: An International Code of Practice for Dosimetry based on Standards of Absorbed Dose to Water.2006 (V.12)

[68]. Burns and Rosser 1990, Havercroft and Klevenhagen 1993.

[69]. Andreo, P.et al. IAEA pubication: Calibration of Photon and Electron Beams.

[70]. P´erez-Calatayud,J. et al. Phantom size in brachytherapy source dosimetric studies. July 2004.

[71]. Granero, D. et al. Equivalent phantom sizes and shapes for brachytherapy dosimetric studies of Ir 192 and Cs 137. Vol. 35, No. 11, November 2008.

[72]. Shakilur, R. et al. Effect of Phantom Material on Backscattered Radiation against Photon Irradiation. RADIOISO- TOPES (Japanese RadioIsotopes Association), Vol. 52 ,2003.

[73]. Bastin, K. et al. The transit dose component of high dose rate brachytherapy: direct measurements and clinical implications. Int J Radiat Oncol Biol Phys. 1993 Jul 15;26(4):695-702.

[74]. Evaluation of measurement data: Guide to the expression of uncertainty in measurement.JCGM,2008.

[75]. Andreo P. et al. On the uncertainties of photon mass energy-absorption coefficients and their ratios for radiation dosimetry. Phys. Med. Biol. 57 (2012) 2117–2136.

[76]. Deutsches Institut fur Normung e.V. [DIN], Terms in the Field of Radiological Technique - Part 3: Dose Quanti- ties and Units. DIN, Berlin, 2001.

[77]. Raffi, A. et al. Determination of exit skin dose for 192Ir intracavitary accelerated partial breast irradiation with thermoluminescent dosimeters, Med. Phys. 37, 2693–2702 .2010.

[78]. Devic, S. et al. Absorption spectra time evolution of EBT-2 model gafchromic film, Med. Phys.37,2010.

[79]. A novel method of radiochromic film dosimetry using a color scanner.Hupe and Brunzendorf, Med. Phys.33,2006. [80]. Song, H. et al. Calculation of brachytherapy doses does not need TG-43 factorization, Med. Phys., 30:6,2003.

[81]. Williamson, F. et al. "Quantitative dosimetry methods for brachytherapy," in Brachytherapy Physics: Joint AAPM/ABS Summer School. Medical Physics,pp. 233– 294.

[82]. Yorke, E. et al..Diode in vivo dosimetry for patients receiving external beam radiation therapy:" AAPM Report No. 87 Medical Physics Publishing, Madison, WI, 2005.

[83]. Zilio, O. et al. Absolute depth-dose-rate measurements for an 192Ir HDR brachytherapy source in water using MOSFET detectors," Med. Phys. 33, 1532–1539. 2006.

[84]. Ramani, R. et al. Clinical dosimetry using MOSFETS. Int. J. Radiat. Oncol., Biol., Phys. 37,1997.

[85]. Beaulieu et al. TG-186: Model-based calculation techniques in brachytherapy. Med. Physic. 39, 2012.